Synthesis of hydrophilic carbon nanotube sponge via post-growth thermal treatment

Luca Camilli[1],*, Daniele Capista[2], Piergiorgio Eramo[2], Angelo Antonio D'Archivio[2], Maria Anna Maggi[3], Andrea Lazzarini[2], Marcello Crucianelli[2], Maurizio Passacantando[2],*

[1] Department of Physics, University of Rome Tor Vergata, Via della Ricerca Scientifica 1, Rome 00133, Italy

[2] Department of Physical and Chemical Sciences, University of L'Aquila, via Vetoio, Coppito, L'Aquila 67100, Italy

[3] Hortus Novus, Via Campo Sportivo 2, Canistro (AQ) 67050, Italy

* E-Mail: luca.camilli@roma2.infn.it; maurizio.passacantando@aquila.infn.it

Clean water is vital for healthy ecosystems, for human life and, in a broader sense, it is directly linked to our socio-economic development. Nevertheless, climate change, pollution and increasing world population will likely make clean water scarcer in the near future. Consequently, it becomes imperative to develop novel materials and more efficient ways of treating waste and contaminated water. Carbon nanotube (CNT) sponges, for example, are excellent in removing oleophilic contaminants; however, due to their super-hydrophobic nature, they are not as efficient when it comes to absorbing water-soluble substances. Here, by means of a scalable method consisting of simply treating CNT sponges at mild temperatures in air, we attach oxygen-containing functional groups to the CNT surface. The functionalized sponge becomes hydrophilic while preserving its micro- and macro-structure and can therefore be used to successfully remove toxic contaminants, such as pesticides, that are dissolved in water. This discovery expands the current range of applications of CNT sponges to those fields in which a hydrophilic character of the sponge is more suitable.

1. Introduction

Carbon nanotube (CNT) sponges are freestanding, macroscopic structures made of self-assembled and interconnected CNTs. The sponges exhibit a density which is comparable to that of the lightest aerogels, and an exceptionally high porosity (>99%) that contributes to give them outstanding elastic and shape-recovery properties.[1,2] In the last ten years, they have been successfully used in a number of applications, for example, in Li-ion batteries[3–6], supercapacitors[7–11], fuel cells[12] and catalysis[13]. Nonetheless, the field in which CNT sponges could provide the most compelling contribution to is probably environmental cleanup, and specifically water purification.

Owing to the intrinsic high specific surface area and super-hydrophobicity, CNTs sponges have shown excellent results when used to purify water from oil, oil-based contaminants or toxic organic chemicals.[1,14–19] Being extremely lightweight and super-hydrophobic, they can float on a body of water and adsorb the hydrophobic contaminants that are polluting its surface. Once the cleanup is over, the monolithic sponges can be easily removed, and the contaminants recovered by gently squeezing the sponge or eliminated by ignition. Either way, the sponge can afterwards be reused for additional cleanup cycles. If it is implemented in a filtration apparatus, a CNT sponge can in fact remove heavy metals and molecular dyes from water as well.[20]

Sometimes, however, it would be more convenient to have hydrophilic sponges that would thus exhibit high wettability with aqueous media. Indeed, in this case they could be employed to remove contaminants and pollutants that are dissolved in water. Additionally, this would potentially eliminate the necessity of inserting the sponge into a filtration apparatus,[20] since hydrophilic sponges would sink into a body of water rather than float on it.

Some research groups have mixed CNT sponges with, for example, polymers in order to create functional composites with hydrophilic properties.[21–23] This, however, comes at the

cost of introducing lengthy and sometimes tedious steps to the synthesis process; more importantly, the presence of a polymer may eventually alter the mechanical and thermal properties of CNT sponges and overall reduces the specific surface area.

Here, we take advantage of the thermal functionalization method in order to produce hydrophilic CNT sponges. This conceptually simple method introduces a mild presence of oxygen-containing functional groups onto the surface of CNTs, especially quinone moieties and ether groups.[24–26] The thermal functionalization is seldom used for CNT powders, where more aggressive but more efficient chemical methods are often preferred (*i.e.*, acid treatments), and has never been applied to the best of our knowledge to CNT sponges before. Furthermore, it is ideal for the sponges because it preserves their monolithic and highly porous structure. We employ a combination of spectroscopic techniques, including Fourier transform-IR (FT-IR) and X-ray photoemission (XPS) spectroscopies in addition to electron microscopy and X-ray diffraction (XRD) to characterize the sponges. Finally, we demonstrate that hydrophilic CNT sponges are indeed more effective than pristine ones (which are super-hydrophobic) when it comes to purifying water from a number of commonly used pesticides.

2. Results and discussions

2.1. Characterization of pristine and hydrophilic CNT sponges

Several CNT sponges with lateral dimensions up to few centimeters are synthesized within an hour by spray pyrolysis chemical vapor deposition method (**Figure 1a**). More details about the synthesis process are given in Experimental section.

As expected, as-grown sponges are super-hydrophobic showing a water contact angle larger than 150 degree (Figure 1b).[27] XRD analysis, shown in Fig. 1c, reveals the typical features of CNTs stemming from the (002) and (101) family of atomic planes in graphite (JCPDS 41-1487). No signal coming from Fe catalyst is detected (neither in its metallic nor in the

3

oxidized form), which is ascribed to the small size of the particles. The presence of Fe within the CNT sponge is nonetheless confirmed by XPS analysis (Supporting Information).
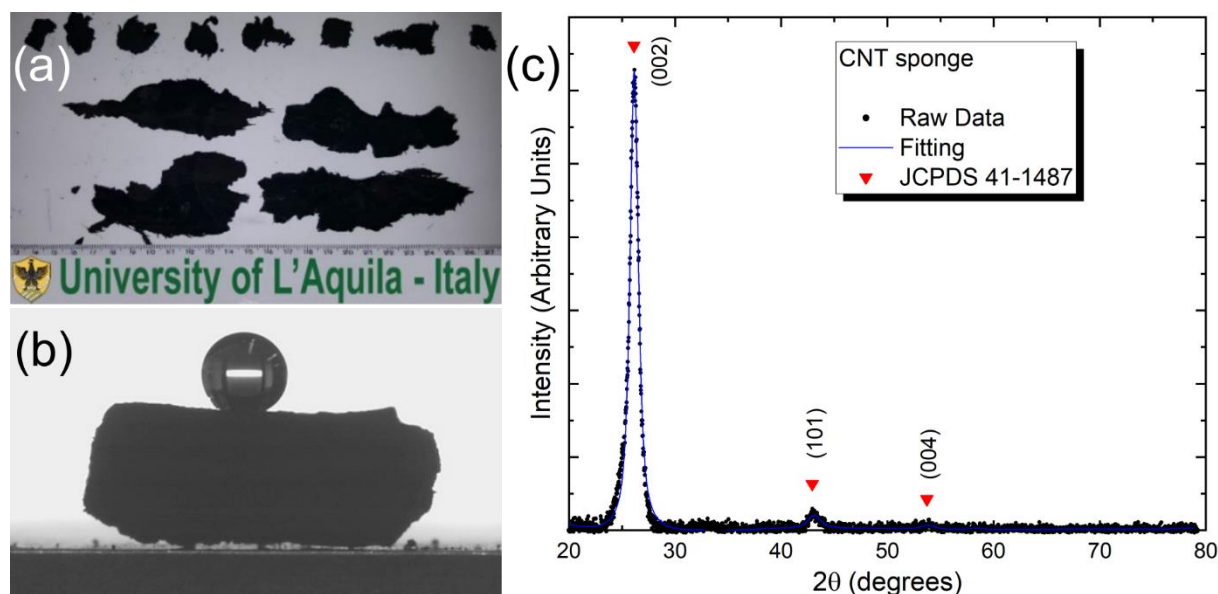

Figure 1. CNT sponges synthesized by spray pyrolysis chemical vapor deposition. (a) Several sponges can be obtained after an hour of synthesis, with the largest ones having up to 10 cm in lateral dimension (b) The static contact angle is 166.5 ° ± 2.2 °. (c) XRD spectrum showing diffraction from the (002) and (101) graphitic planes of the CNTs (JCPDS 41-1487).

In order to make the sponges hydrophilic, a mild thermal treatment at 450 °C for 1 h in air was carried out. The temperature of 450 °C was selected on the basis of previous studies concerning thermal stability of CNT powders showing that a mild oxidation reaction does occur in air between 440 °C and 465 °C.[24,26]

The microscopic structure of both as-grown and thermally treated CNT sponges as investigated by scanning electron microscopy (SEM) is displayed in **Figure 2**. From this analysis, we can infer that the thermal treatment does not alter the overall sponge microstructure in a significant way. Although the average diameter of the tubes seems to be slightly reduced after the thermal treatment (see the Inset in Figure 2), both samples still look very similar, consisting of a large amount of randomly oriented and entangled CNTs. More specifically, two types of tubes are present; some are straighter and have diameters in excess of hundreds of nanometers, whereas others are much thinner, highly twisted and bent. Here, it

is worth highlighting that the presence of such twisted and highly defected CNTs is indeed

essential to create an interconnected network, as discussed in previous works.[1,28,29] In fact, it

will be discussed later that the presence of defects is what makes functionalization by thermal

treatment so efficient in the case of CNT sponges.
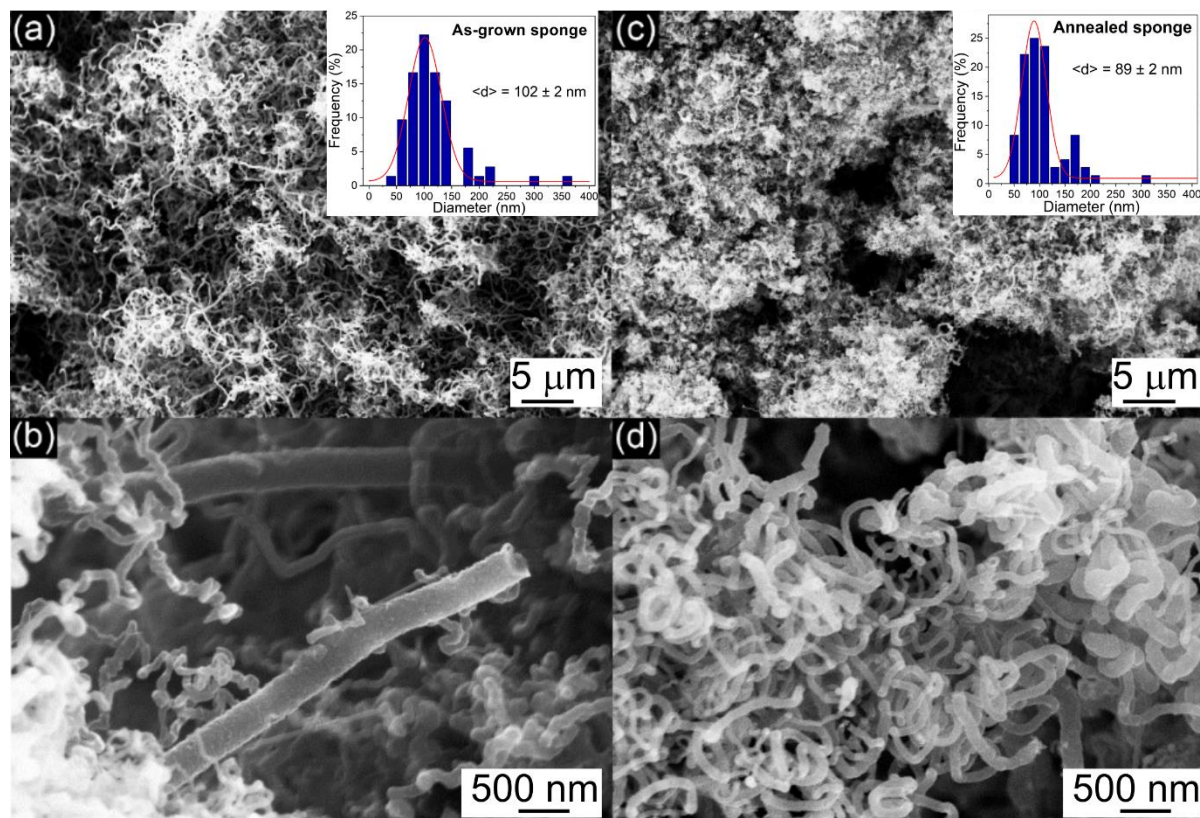
Figure 2. Analysis of the microstructure of as-grown and annealed CNT sponges. SEM
micrographs of CNT sponges before (a, b) and after (c, d) thermal treatment at 450 °C for 1h
in air. Insets: diameter distribution of CNTs making up the as-grown sponge (a) and the
annealed one (b). In both cases, while the majority of the tubes is distributed along a
Gaussian peaked at around 100 nm for the as-grown sample and 90 nm for the annealed on, a
small fraction of tubes has larger diameters (in excess of 150 nm).

To verify that the thermal treatment effectively introduces functional groups onto the surface

of the CNTs constituting the sponge, FT-IR spectroscopy measurements have been performed

on the samples prior to and after the thermal treatment. FT-IR spectra for as-grown (black

curve) and annealed (red curve) CNT sponges are displayed in **Figure 3a**.
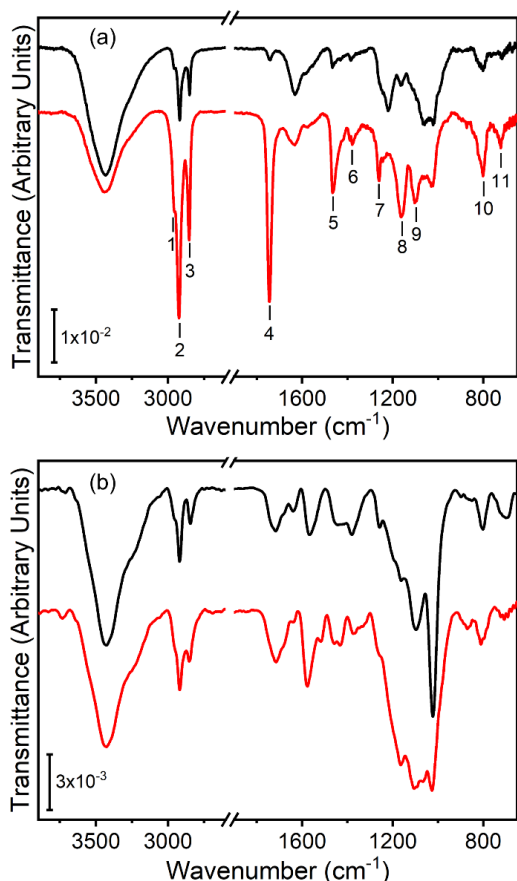
Figure 3. FT-IR characterization. (a) FT-IR spectra of as-grown (black curve) and thermally treated (red curve) CNT sponges. Band numbering refers to peak assignation as reported in Table 1. (b) FT-IR spectra of commercial CNT powder before (black curve) and after (red curve) annealing at 450 °C for 1 h in air are reported for comparison. Both in (a) and (b), the two curves are vertically shifted for visualization purposes, while the break between 2600 and 1900 cm^{-1} is meant to exclude a part of the spectra with no IR absorption features.

Table 1. List of the principal functional groups present on the surface of as-grown and annealed CNT sponges and their relative IR frequencies.

Chemical species	Frequency [cm^{-1}]	Type of vibration	Numeration[a]
Aliphatic species	2960	$\nu(CH_3)$	1
	2920	$\nu_{as}(CH_2)$	2
	2850	$\nu_s(CH_2)$	3
	1465	$\delta_{as}(CH_2)$	5
	1357	$\delta_s(CH_2)$	6
	800	$\omega(CH_2)$	10
	720	$\tau(CH_2)$	11
Lactones	1740	$\nu(C=O)$	4
	1260	$\delta_{as}(C-O-C)$	7
	1100	$\delta_s(C-O-C)$	9
Phenols	1165	$\delta(OH)$	8

a) Follow numeration in Figure 3a.

6

Both spectra feature signals arising from a wide variety of different chemical species (for a list of the functional groups and their relative IR frequency peaks, see **Table 1**). Notably, due to the high specific surface area of the samples, signals from physisorbed moisture are present in both samples. This is evident from the broad and intense band centered at 3450 cm^{-1}, due to -OH stretching mode, and from a weaker and narrower signal at 1625 cm^{-1} coming from -H-O-H scissoring mode.[30,31] Moreover, both samples present signals typical of extensively aromatic samples, such as C-C$_{arom}$ stretching at 1590 cm^{-1} (visible as shoulder of 1625 cm^{-1} peak),[32] and different in-plane (1220 cm^{-1}) and out-of-plane (1065, 1020 and 800 cm^{-1}) modes of aromatic C-H species[33] arising from defects in the graphitic structure of CNTs. Defects in the extended sp^2 conjugated structure of CNTs sponges may be due to aliphatic dangling groups, giving rise to the three signals at 2960, 2920 and 2850 cm^{-1}.[34] In addition to revealing the presence of the above mentioned groups that are common in both samples, FT-IR analysis also clearly shows that the thermal annealing in air does lead to a controlled insertion of oxygenated groups at expenses of the graphitic structure. Specific bands in the IR spectrum are indeed much more intense in the thermally treated sample. The main of these bands are related to the presence of cyclic esters, more precisely the very intense and sharp peak at 1740 cm^{-1} due to C=O stretching of lactones, coupled with the antisymmetric and symmetric stretching of the C-O-C species in lactones (1260 and 1100 cm^{-1} respectively).[32,35] Another abundant species appearing after the thermal annealing process are phenols, identified with the band at 1165 cm^{-1}.[36] A further consequence of the thermal treatment, apart from the insertion of oxygenated groups onto the surface of the CNT sponges, is the increasing rupture of the conjugated sp^2 structure, promoting the growth of linear saturated hydrocarbons, justifying the consistent growth of C-H stretching in the 2960-2850 cm^{-1} range, C-H bending at 1465 and 1357 cm^{-1} and C-H wagging at 800 and 720 cm^{-1}.[34]

For comparison purposes, commercial multi-wall CNTs (Sigma Aldrich) were also treated in air at 450 °C for 1 h. The corresponding FT-IR spectra of pristine and annealed samples are shown in Figure 4b. Overall, it is possible to observe the same spectral features already observed for the CNTs sponges (Figure 4a). However, it is clear that the thermal treatment performed on the CNT powder does not lead to the same dramatic change in the amount of oxygen-containing functional groups that was observed for the CNT sponges, exception made for the creation of phenolic groups (signal at ~1150 cm^{-1}) due to the probable functionalization of randomly located defects or amorphous carbon in the main carbon nanotube texture.[37] We explain the different behavior of our CNT sponges and the commercial CNT powder as due to the larger number of structural defects that are present in the former. In other words, the higher quality of the commercial CNTs make them more inert. This last statement is obvious, given the well-known inertness of C sp^2 lattice, and is the reason why chemical, hence more aggressive, methods are preferred to functionalize CNTs rather than thermal annealing.[38–40]

For a more quantitative characterization of the functional groups present on the CNT sponges, we rely on XPS analysis. Normalized C 1s core levels of as-grown and thermally treated sponges are reported in **Figure 4a and b**, respectively. The peaks are fitted by the sum of five components assigned to different bonding configurations of C atoms (in line with Ref. [41–43]) and the π- π* shake up satellite (291.1 eV). These components belong to aromatic rings carbon (C=C/C-C/C-H, 284.8 eV), hydroxyl groups (C-OH, 258.9 eV), epoxy groups (C-O-C, 286.9 eV), carbonyl groups (C=O, 288.2 eV) and carboxyl groups (C=O(OH), 289.3 eV). The relative abundance of each component of the C 1s spectra is reported in **Table 2**. It is evident that all the oxygen-containing groups increase significantly in intensity upon annealing, while the aromatic group component decreases. Notably, the main increase is

found for the carbonyl and carboxyl groups, which increase by a factor 3 and 1.68, respectively, followed by the epoxy group, which increases by a factor 1.4. These results are consistent with those obtained from FT-IR measurements (Figure 3a).
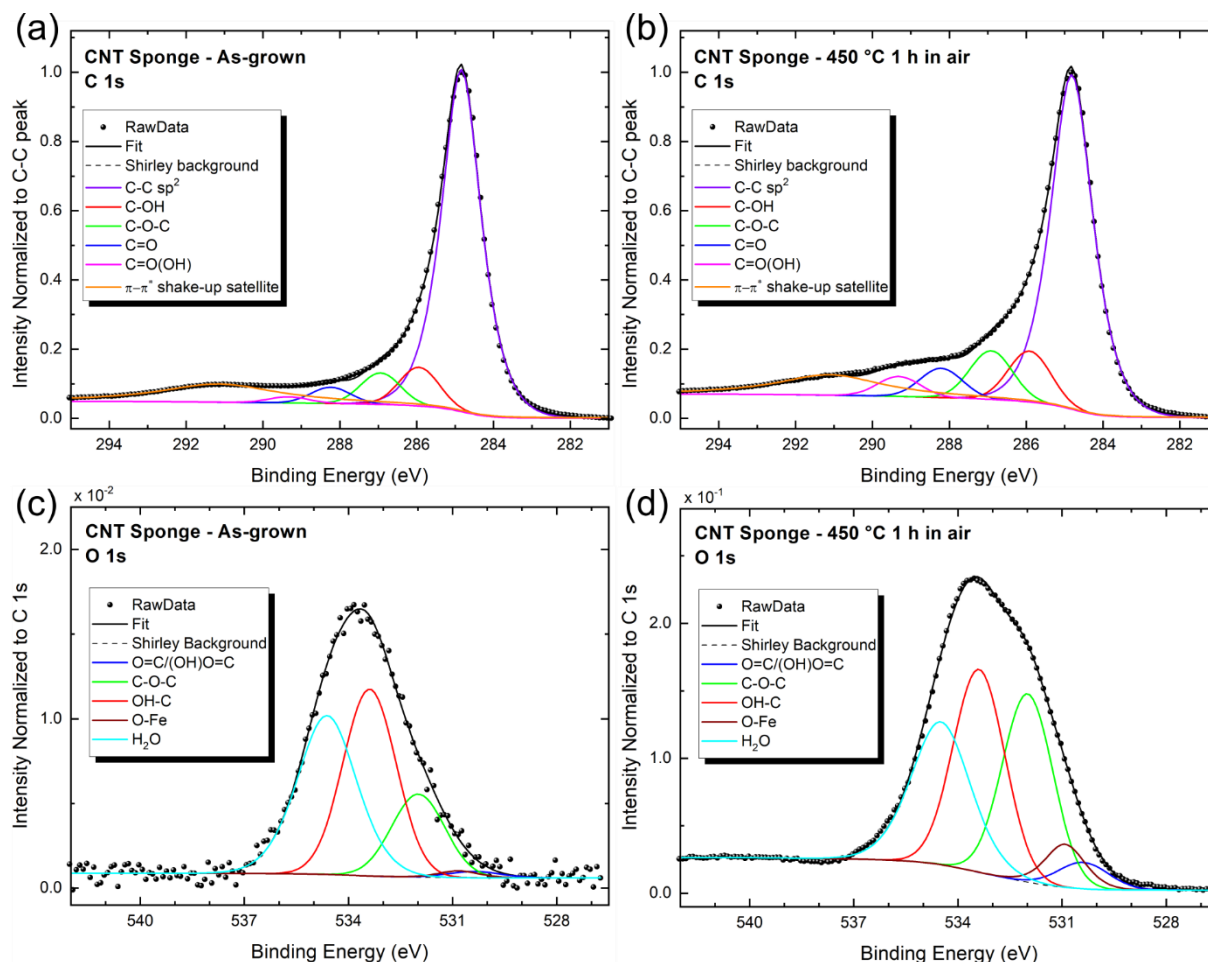
Figure 4. XPS characterization of as-grown and thermally treated CNT sponge. (a, b) C 1s and (c, d) O 1s core levels. Both the experimental data and the fits after background removal are shown.

Table 2. Percentage of the functional groups as obtained from fitting C 1s core level as shown in Figure 4a and b.

Sample	C-C sp^2 [%]	C-OH [%]	C-O-C [%]	C=O [%]	C=O(OH) [%]
As-grown	80.4	8.2	6.7	3.4	1.3
Thermally treated	71.1	9.9	9.4	5.7	3.9

Direct evidence of the effect of the thermal treatment on the physico-chemical properties of CNT sponges is presented in **Figure 5**. While the as-grown sponge floats on the water surface

due to its super-hydrophobicity (left), the thermally treated one sinks as a result of its
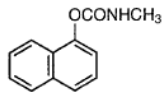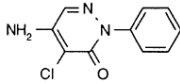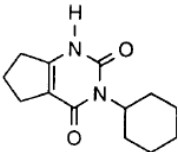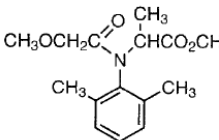
hydrophilic character (right).

Figure 5. Evidence of the hydrophilic nature of thermally treated CNT sponges. While an as-grown sponge floats on water (left), a sponge annealed in air at 450 °C for 1 h sinks at the bottom of the water-filled cuvette (right).

2.2. Adsorption of contaminants from water

A wide range of synthetic chemicals is used in agriculture to keep insects, weeds, fungi and

other pests under control, ultimately increasing crop production and reducing postharvest

losses. Furthermore, some of these chemicals are also used in home gardens, in forestry and

rangeland protection, and for maintenance of sports arenas.[44,45] As a consequence, they are

now present as contaminants in terrestrial and aquatic environments all over the world,[46–48]

thus posing serious health concerns for humans and animals alike.[49–52] It is therefore

necessary to develop efficient approaches for removal of such contaminants.

Owing to their hydrophilic character, thermally treated CNT sponges are supposed to exhibit

a higher efficiency in removing soluble contaminants from water when compared to as-

grown, super-hydrophobic CNT sponges. To demonstrate this, here we used both thermally

treated and as-grown CNT sponges as adsorbent materials for the uptake of four commonly

used pesticides (i.e., carbaryl, lenacil, metalaxyl and chloridazon) from water. The chemical

formula and main properties of the target pesticides are displayed in **Table 3**.

Table 3. Main properties and use of the investigated pesticides.

| Name	IUPAC name	Class, use	Structural formula	S (mg/L)[a]	pK$_{ow}$[b]
Carbaryl	1-Naphthyl-N-methylcarbamate	carbamate, insecticide		9.1	2.36
Chloridazon	5-Amino-4-chloro-2-phenylpyridazin-3(2H)-one	pyridazinone, herbicide		422	1.19
Lenacil	3-Cyclohexyl-1,5,6,7-tetrahydrocyclopentapyrimidine-2,4(3H)-dione	uracil, herbicide		2.9	1.69
Metalaxyl	Methyl 2-[(2,6-dimethylphenyl)(methoxyacetyl)amino]propanoate	phenylamide, fungicide		8400	1.75

[a] Solubility in water; [b] logarithm of octanol/water partition coefficient [53]

Carbaryl, an insecticide belonging to the class of carbamates, is one of the most widely used pesticides in the world and is potentially harmful for environment and humans.[54] Human toxicity from carbaryl has been documented in workers engaged in its packaging and in farmers.[55] This insecticide has been included in the priority blacklist released by the US Environmental Protection Agency (EPA) because of its potential carcinogenic and mutagenic action.[56] Chloridazon is a selective herbicide for control of annual broad-leaved weeds, exhibiting a moderate persistence and high mobility in soils. It has been detected, together with its degradation products, in surface water and groundwater, often at concentration levels above the EU limits, posing potential risks to aquatic organisms and human health.[57–59] Lenacil is the active substance in many herbicide products. According to the European Chemical Agency (ECHA), lenacil is very toxic to aquatic life and is suspected of causing cancer.[60] Metalaxyl is a broad-spectrum fungicide used to prevent or combat fungal diseases in fruits, vegetables, and cereal crops. Because of its extensive use in agriculture, along with its high stability and solubility in water, metalaxyl can contaminate

groundwater and surface runoff.[61] Residuals of metalaxyl have been frequently found in food samples, therefore, it is likely that this pesticide reaches humans through the food chain. It exhibits toxicological effects.[55], [62]

The results of the adsorption experiments are presented in **Figure 6**. It is evident that the annealed CNT sponge is indeed a superior adsorbent material as it shows an uptake that compared to that one of as-grown sponges is larger by a factor approximately 1.5, 1.7, 9 and 1.7 for carbaryl, lenacil, metalaxil and chloridazon, respectively. Because of the aromatic character of all the target pesticides combined with the graphite-like structure of nanotubes, π-π interaction should be regarded as the main intermolecular force responsible for the absorption of the above chemicals on the sponges. Nevertheless, annealing in air introduces hydrophilic groups on the nanotube surface, therefore, polar (dipole-dipole or hydrogen bonding) interactions can also have a role in determining the adsorption properties of the annealed sponges. Apart from the effects on the interaction mechanism at molecular level, hydrophilic functionalization of the sponges improves wettability of the material, and, therefore, increases the extension of water-sorbent interphase were absorption phenomena take place. Here, it is worth discussing the case of metalaxyl, as it is the component for which the adsorption difference between annealed and as-grown sponge is the largest, by far. The explanation is indeed quite simple; among the four chemicals used in this study, metalaxyl is the one with the highest hydrophilic character (its solubility in water, for example, is orders of magnitude larger than that of the other chemicals considered here). This also explains why as-grown CNT sponges, being super-hydrophobic, have a negligible uptake capacity towards it. The enhanced adsorption capability of metalaxyl on the annealed sponges can be explained by introduction of hydroxyl and carboxyl groups able to interact via hydrogen bonding with the O and N atoms of metalaxyl, acting as hydrogen-bond acceptors. On the other hand, carbaryl, which has a distinct hydrophobic character and a low solubility in water, is the one most

12

efficiently adsorbed among the four investigated pesticides by both pristine and annealed sponges. Moreover, it can be pointed out that the annealing process leads to a noticeably lower uptake improvement compared to that of metalaxyl. These findings can be explained by the dominant role of the π-π intermolecular interactions, whereas the moderate increase in the uptake of carbaryl on the annealed sponges seems to be the consequence of the improved wettability of the sponges after annealing.
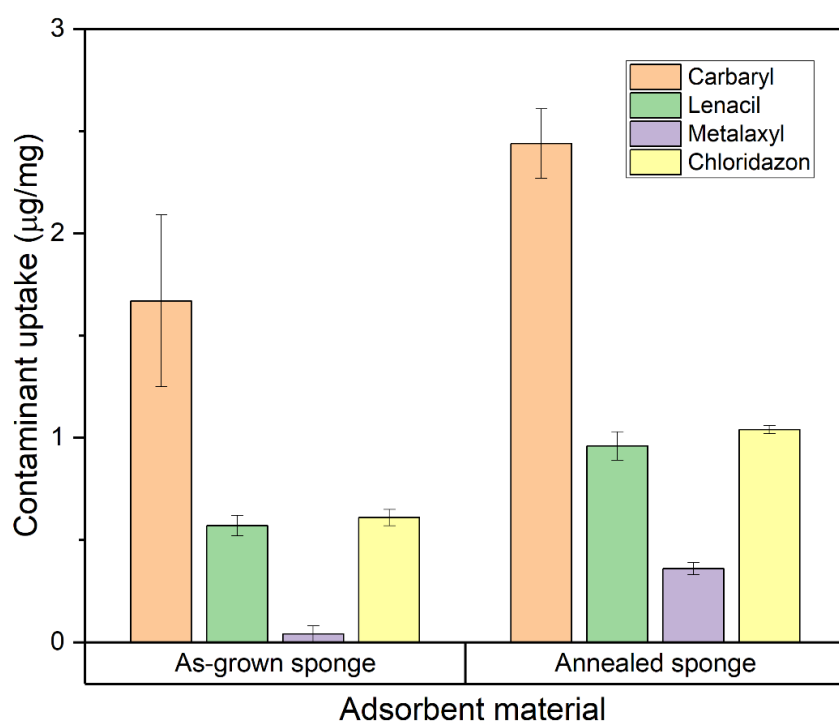
Figure 6. Contaminant uptake. Histogram comparing the uptake of four pesticides (carbaryl, lenacil, metalaxyl, chloridazon) by as-grown (left side) and annealed (right side) sponges. Error bars are shown.

3. Conclusion

In this work, we have shown that a mild thermal treatment carried out in air at ambient pressure introduces oxygen-containing functional groups on the surface of CNTs, thus transforming CNT sponges from super-hydrophobic to hydrophilic. It is worth highlighting that this method is scalable, because there is no limit to the amount of sponges that can be treated this way (except the volume of the oven), and that it does not require use of chemicals but simply high temperature and air. Depending on the application, hydrophilic sponges may

be more desirable than super-hydrophobic ones. Indeed, as they show a larger wettability to water, they should be more efficient in those applications in which the sponge is in contact with an aqueous solution, for example in the case of fuel cells. Similarly, it should be easier to further modify them via wet chemistry. Here, we have demonstrated that hydrophilic CNT sponges are indeed better than as-grown ones at adsorbing water-soluble contaminants from aqueous solution. The contaminants considered here are commonly used pesticides, nominally carbaryl, lenacil, metalaxyl, chloridazon, that are considered toxic to either the environment or humans or both. Finally, the results presented here will likely expand the range of applications of CNT sponges to those fields in which a hydrophilic character of the sponge is more suitable.

4. Experimental Section/Methods

Synthesis of pristine CNT sponges: The CNT sponges were grown by spray pyrolysis-chemical vapor deposition (SP-CVD) method in a tube furnace with a spraying setup. More details about the setup are given in Supporting Information. Before starting the growth, the reactor was pumped down to below 10^{-5} Torr using a turbo molecular pump. After reaching the growth temperature, T=1000 °C, in the center of the furnace, the reactor was filled with Argon up to ambient pressure (760 Torr).

Ferrocene (2.3 wt%) and thiophene (1.5 wt%), respectively used as catalyst and growth enhancer, were dissolved in ethanol and the precursor solution was stirred overnight. During growth, the solution was injected through a thin outlet outside the reactor via a pump syringe at a constant rate of 7.5 ml h^{-1} in a mixture of Ar:C_2H_2 (400:200 sccm), which act as carrier gas and carbon precursor, respectively. The injection point was 300 mm away from the end plate of the reactor with local temperature of about 450 °C. In these conditions the injected solvent was instantly vaporized at the end of the outlet and finely dispersed into the carrier gas flow.

14

Thermal functionalization of CNT sponges: The thermal functionalization was carried out in an oven (in air ambient) for 1 h at 450 °C with a heating rate of 7 °C min^{-1}.

Structural and chemical characterization of pristine and functionalized CNT sponges: The crystalline structure was examined by using a Bruker D-5000 X-ray diffraction (XRD) system with Cu Kα radiation.

The morphology was studied with a Zeiss - Gemini Leo 1530 field emission scanning electron microscope operating with an accelerating voltage of 10 kV. An in-lens detector was used.

The contact angle was measured with a Krüss DSA100 system, dropping about 1 μL (1-2 mm of diameter) of distilled water on the sample with a micro syringe and acquiring the cross-sectional image of the drop.

FT-IR spectra were collected by means of a VERTEX70v instrument by Bruker equipped with a DTGS detector in the Mid-IR region. Each spectrum was collected by averaging 256 scans with a resolution of 4 cm^{-1}. Due to the strong scattering of light by CNTs, only a minimal amount of the sponges was mixed with KBr (previously treated at 300 °C for 1 h and kept inside a desiccant box afterwards) and ground together using an agate mortar. The obtained fine powder mix was pressed into a pellet and measured in transmission mode under dynamic vacuum conditions.

XPS was carried out using a PHI 1257 system (Physical Electronics) at a base pressure of 10^{-9} Torr. Each sample was analyzed using a non-monochromatic Al Kα X-ray source (hν = 1486.6 eV) at a power of 300 W, with the analyzer being operated in constant energy mode at a pass energy of 190 eV for the survey spectra and 20 eV for the high-resolution scans. Quantitative surface analyses were calculated from peak areas, using the appropriate instrument modified sensitivity factors. For the fit, the XPS core-level peaks were

deconvoluted into various components using mixed Gaussian-Lorentzian curves and an interactive least-squares computer program.

Pesticide adsorption: Adsorption of pesticides on the CNT sponges was investigated by putting in contact the material (5 mg) with 1 mL of an aqueous solution of each pesticide at a concentration of 30 mg/L, kept at room temperature in static conditions for 3 h. Then the CNT sponge was removed, a suitable aliquot of the aqueous solution was collected, filtered, and analyzed by high-performance liquid chromatography (HPLC). Preliminary experiments ensured that the adsorption equilibrium was reached in this condition. The amount q of each pesticide adsorbed on the CNT sponge was determined according to the following relationship:

$$q = (C_0 - C_{eq})V/m \qquad (1)$$

where C_0 and C_{eq} are the initial and equilibrium concentrations, respectively, V the volume of solution and m the mass of adsorbent.

The HPLC measurements were performed by a Waters chromatographic system (Waters, Milford, MA, USA) consisting of a Model 600 pump, a 600 Pump Controller Module, an Acqua 717 plus auto-sampler, and a 996 photodiode array detector. Chromatographic data management was automated using the Empower data acquisition system (Waters). The analyses were carried on a 250×4.6 mm analytical column Sinergy (Phenomenex, Torrance, CA, USA) with 4 μm particle size connected to a 4×3mm UHPLC guard cartridge (Phenomenex) with 5 μm particle size. The eluent, consisting of a water-acetonitrile 50:50 % (v/v) mixture, was degassed by an Agilent 1200 system (Agilent Technologies, Waldbronn, Germany) and supplied at a flow rate of 1.0 mL/min. Five-point calibration curves in water, covering the concentration range 1-50 mg/L (R^2 better than 0.992), were built for each pesticide by dilution of stock solutions previously prepared by dissolving 10 mg of each

compound in 10 mL of acetonitrile. Analytical standards of the investigated pesticides

(purity>99%) were acquired from Sigma Aldrich (St. Louis, MO, USA).

References

[1]   X. Gui, J. Wei, K. Wang, A. Cao, H. Zhu, Y. Jia, Q. Shu, D. Wu, *Adv. Mater.* **2010**, *22*, 617.

[2]   Z. Lin, Z. Zeng, X. Gui, Z. Tang, M. Zou, A. Cao, *Adv. Energy Mater.* **2016**, *6*, 1.

[3]   Y.-S. Liu, C. Ma, Y.-L. Bai, X.-Y. Wu, Q.-C. Zhu, X. Liu, X.-H. Liang, X. Wei, K.-X. Wang, J.-S. Chen, *J. Mater. Chem. A* **2018**, *6*, 17473.

[4]   M. Zou, Z. Ma, Q. Wang, Y. Yang, S. Wu, L. Yang, S. Hu, W. Xu, P. Han, R. Zou, A. Cao, *J. Mater. Chem. A* **2016**, *4*, 7398.

[5]   L. Hu, H. Wu, Y. Gao, A. Cao, H. Li, J. McDough, X. Xie, M. Zhou, Y. Cui, *Adv. Energy Mater.* **2011**, *1*, 523.

[6]   Y. Shen, D. Sun, L. Yu, W. Zhang, Y. Shang, H. Tang, J. Wu, A. Cao, Y. Huang, *Carbon N. Y.* **2013**, *62*, 288.

[7]   X. Cheng, X. Gui, Z. Lin, Y. Zheng, M. Liu, R. Zhan, Y. Zhu, Z. Tang, *J. Mater. Chem. A* **2015**, *3*, 20927.

[8]   P. Li, C. Kong, Y. Shang, E. Shi, Y. Yu, W. Qian, F. Wei, J. Wei, K. Wang, H. Zhu, A. Cao, D. Wu, *Nanoscale* **2013**, *5*, 8472.

[9]   X. Yang, X. He, Q. Li, J. Sun, Z. Lei, Z.-H. Liu, *Energy & Fuels* **2021**, DOI 10.1021/acs.energyfuels.0c03745.

[10]   P. Li, Y. Yang, E. Shi, Q. Shen, Y. Shang, S. Wu, J. Wei, K. Wang, H. Zhu, Q. Yuan,

A. Cao, D. Wu, *ACS Appl. Mater. Interfaces* **2014**, *6*, 5228.

[11] X. Cao, J. He, H. Li, L. Kang, X. He, J. Sun, R. Jiang, H. Xu, Z. Lei, Z. H. Liu, *Small* **2018**, *14*, 1.

[12] C. Erbay, G. Yang, P. De Figueiredo, R. Sadr, C. Yu, A. Han, *J. Power Sources* **2015**, *298*, 177.

[13] Y. Wang, Y. Liu, T. Liu, S. Song, X. Gui, H. Liu, P. Tsiakaras, *Appl. Catal. B Environ.* **2014**, *156–157*, 1.

[14] X. Li, Y. Xue, M. Zou, D. Zhang, A. Cao, H. Duan, *ACS Appl. Mater. Interfaces* **2016**, *8*, 12337.

[15] L. Camilli, C. Pisani, E. Gautron, M. Scarselli, P. Castrucci, F. D'Orazio, M. Passacantando, D. Moscone, M. De Crescenzi, *Nanotechnology* **2014**, *25*, DOI 10.1088/0957-4484/25/6/065701.

[16] K. Zhu, Y. Y. Shang, P. Z. Sun, Z. Li, X. M. Li, J. Q. Wei, K. L. Wang, D. H. Wu, A. Y. Cao, H. W. Zhu, *Front. Mater. Sci.* **2013**, *7*, 170.

[17] D. Kukkar, A. Rani, V. Kumar, S. A. Younis, M. Zhang, S. S. Lee, D. C. W. Tsang, K. H. Kim, *J. Colloid Interface Sci.* **2020**, *570*, 411.

[18] A. J. Cortés-López, E. Muñoz-Sandoval, F. López-Urías, *ACS Omega* **2019**, *4*, 18011.

[19] Y. Lu, W. Yuan, *ACS Appl. Mater. Interfaces* **2017**, *9*, 29167.

[20] H. Li, X. Gui, L. Zhang, S. Wang, C. Ji, J. Wei, K. Wang, H. Zhu, D. Wu, A. Cao, *Chem. Commun.* **2010**, *46*, 7966.

[21] W. Zhan, L. Gao, X. Fu, S. H. Siyal, G. Sui, X. Yang, *Appl. Surf. Sci.* **2019**, *467–468*, 1122.

[22] F. Zhang, Y. Feng, M. Qin, L. Gao, Z. Li, F. Zhao, Z. Zhang, F. Lv, W. Feng, *Adv. Funct. Mater.* **2019**, *29*, 1.

[23] Y. Wu, Y. Wang, Z. Lin, Y. Wang, Y. Li, S. Liu, X. Gui, X. Yang, *Sep. Purif.*

Technol. **2019**, *211*, 359.

[24]   K. Behler, S. Osswald, H. Ye, S. Dimovski, Y. Gogotsi, *J. Nanoparticle Res.* **2006**, *8*, 615.

[25]   S. Yang, X. Wang, H. Yang, Y. Sun, Y. Liu, *J. Hazard. Mater.* **2012**, *233–234*, 18.

[26]   X. Chen, X. Z. Tang, Y. N. Liang, J. W. Cheah, P. Hu, X. Hu, *J. Mater. Sci.* **2016**, *51*, 5625.

[27]   R. E. Johnson, *Contact Angle, Wettability, and Adhesion*, Am. Chem. Soc., **1964**.

[28]   L. Camilli, C. Pisani, M. Passacantando, V. Grossi, M. Scarselli, P. Castrucci, M. De Crescenzi, *Appl. Phys. Lett.* **2013**, *102*, DOI 10.1063/1.4804385.

[29]   D. P. Hashim, N. T. Narayanan, J. M. Romo-Herrera, D. A. Cullen, M. G. Hahm, P. Lezzi, J. R. Suttle, D. Kelkhoff, E. Muñoz-Sandoval, S. Ganguli, A. K. Roy, D. J. Smith, R. Vajtai, B. G. Sumpter, V. Meunier, H. Terrones, M. Terrones, P. M. Ajayan, *Sci. Rep.* **2012**, *2*, 1.

[30]   K. Krishnamoorthy, R. Mohan, S. J. Kim, *Appl. Phys. Lett.* **2011**, *98*, 2009.

[31]   T. Li, C.-Z. Zhang, X. Fan, Y. Li, M. Song, *Chem. Eng. J.* **2017**, *323*, 37.

[32]   K. Kobashi, Y. Iizumi, K. Hirota, N. Shinomori, K. Shimamoto, Y. Koga, T. Morimoto, T. Okazaki, *ACS Appl. Nano Mater.* **2021**, *4*, 5273.

[33]   A. Piovano, A. Lazzarini, R. Pellegrini, G. Leofanti, G. Agostini, S. Rudić, A. L. Bugaev, C. Lamberti, E. Groppo, *Adv. Condens. Matter Phys.* **2015**, *2015*, DOI 10.1155/2015/803267.

[34]   A. R. Sadrolhosseini, M. Habibiasr, H. Soleimani, M. N. Hamidon, Y. W. Fen, H. N. Lim, *J. Sensors* **2021**, *2021*, DOI 10.1155/2021/8813801.

[35]   A. Lazzarini, R. Pellegrini, A. Piovano, S. Rudić, C. Castan-Guerrero, P. Torelli, M. R. Chierotti, R. Gobetto, C. Lamberti, E. Groppo, *Catal. Sci. Technol.* **2017**, *7*, 4162.

[36]   L. Stobinski, B. Lesiak, L. Kövér, J. Tóth, S. Biniak, G. Trykowski, J. Judek, *J. Alloys*

Compd. **2010**, *501*, 77.

[37]   J. M. Moon, K. H. An, Y. H. Lee, Y. S. Park, D. J. Bae, G. S. Park, *J. Phys. Chem. B* **2001**, *105*, 5677.

[38]   N. Sezer, M. Koç, *Surfaces and Interfaces* **2019**, *14*, 1.

[39]   J. Chen, Q. Chen, Q. Ma, *J. Colloid Interface Sci.* **2012**, *370*, 32.

[40]   L. Thi Mai Hoa, *Diam. Relat. Mater.* **2018**, *89*, 43.

[41]   S. Stankovich, D. A. Dikin, R. D. Piner, K. A. Kohlhaas, A. Kleinhammes, Y. Jia, Y. Wu, S. T. Nguyen, R. S. Ruoff, *Carbon N. Y.* **2007**, *45*, 1558.

[42]   A. A. D'Archivio, M. A. Maggi, A. Odoardi, S. Santucci, M. Passacantando, *Nanotechnology* **2018**, *29*, 65701.

[43]   S. Park, K.-S. Lee, G. Bozoklu, W. Cai, S. T. Nguyen, R. S. Ruoff, *ACS Nano* **2008**, *2*, 572.

[44]   J. Popp, K. Pető, J. Nagy, *Agron. Sustain. Dev.* **2013**, *33*, 243.

[45]   I. Md Meftaul, K. Venkateswarlu, R. Dharmarajan, P. Annamalai, M. Megharaj, *Sci. Total Environ.* **2020**, *711*, 134612.

[46]   F. P. Carvalho, *Food Energy Secur.* **2017**, *6*, 48.

[47]   N. Cuevas, M. Martins, P. M. Costa, *Ecotoxicology* **2018**, *27*, 1008.

[48]   A. Mojiri, J. L. Zhou, B. Robinson, A. Ohashi, N. Ozaki, T. Kindaichi, H. Farraji, M. Vakili, *Chemosphere* **2020**, *253*, 126646.

[49]   A. Sabarwal, K. Kumar, R. P. Singh, *Environ. Toxicol. Pharmacol.* **2018**, *63*, 103.

[50]   P. C. Jepson, K. Murray, O. Bach, M. A. Bonilla, L. Neumeister, *Lancet Planet. Heal.* **2020**, *4*, e56.

[51]   M. R. Bonner, M. C. R. Alavanja, *Food Energy Secur.* **2017**, *6*, 89.

[52]   H. Siviter, E. J. Bailes, C. D. Martin, T. R. Oliver, J. Koricheva, E. Leadbeater, M. J. F. Brown, *Nature* **2021**, *596*, 389.

[53] "PPDB: Pesticide Properties DataBase, University of Hertfordshire (UK)," **n.d.**

[54] M. G. Lee, V. Patil, Y. C. Na, D. S. Lee, S. H. Lim, G. R. Yi, *Sensors Actuators, B Chem.* **2018**, *261*, 489.

[55] Q. Saquib, M. A. Siddiqui, S. M. Ansari, H. A. Alwathnani, J. Musarrat, A. A. Al-Khedhairy, *J. Appl. Toxicol.* **2021**, *41*, 832.

[56] F. Shahdost-fard, N. Fahimi-Kashani, M. R. Hormozi-nezhad, *Talanta* **2021**, *221*, 121467.

[57] J. Velisek, A. Stara, E. Zuskova, J. Chabera, J. Kubec, M. Buric, A. Kouba, *Chemosphere* **2020**, *257*, 127189.

[58] J. Chabera, A. Stara, J. Kubec, M. Buric, E. Zuskova, A. Kouba, J. Velisek, *Ecotoxicol. Environ. Saf.* **2021**, *208*, 111645.

[59] M. Fernández-Pérez, M. Villafranca-Sánchez, F. Flores-Céspedes, S. Pérez-García, I. Daza-Fernández, *Environ. Pollut.* **2010**, *158*, 1412.

[60] J. Chmist, K. Szoszkiewicz, D. Drożdżyński, *Arch. Environ. Contam. Toxicol.* **2019**, *77*, 432.

[61] A. S. H. Derbalah, A. El-Banna, M. Saad Allah, *Curr. Microbiol.* **2020**, *77*, 2991.

[62] E. K. Matich, J. A. Laryea, K. A. Seely, S. Stahr, L. J. Su, P. C. Hsu, *Ecotoxicol. Environ. Saf.* **2021**, *219*, 112327.

Supplementary Data

Synthesis of hydrophilic carbon nanotube sponge via post-growth thermal treatment

Luca Camilli, Daniele Capista, Piergiorgio Eramo, Angelo Antonio D'Archivio, Maria Anna Maggi, Andrea Lazzarini, Marcello Crucianelli, Maurizio Passacantando

Additional details about the synthesis setup

The setup for the synthesis of CNT sponges consists of a tube furnace (length 600 mm) with effective heating length of 100 mm in the center, a quartz reactor tube (i.d. 50 mm, length 1000 mm), and a spraying setup, as schematically shown in **Figure S1**. The device developed for spraying liquids injected at low flow rates consists of a carrier gas tube (i.d. 4.2 mm) which ends with a spraying nozzle (i.d. 0.5 mm) and a sealed inner tube (i.d. 1.5 mm) that carries the solution. The pressure formed inside the carrier gas tube ensures that the solution is finely vaporized at low flow rates through the nozzle.
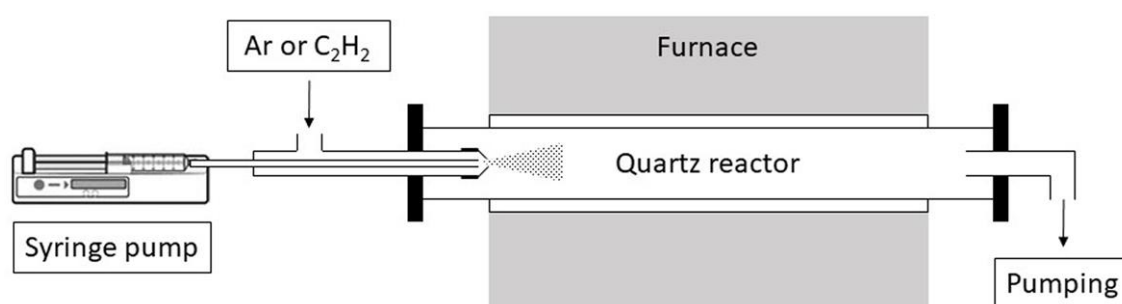

Figure S1. Scheme of the experimental setup used for the synthesis of CNT sponges.

Analysis of Fe 2p core level

XPS analysis of the Fe 2p core level is reported in **Figure S2** for as-grown and thermally treated sponges. In both cases, Fe is oxidized to some degree.
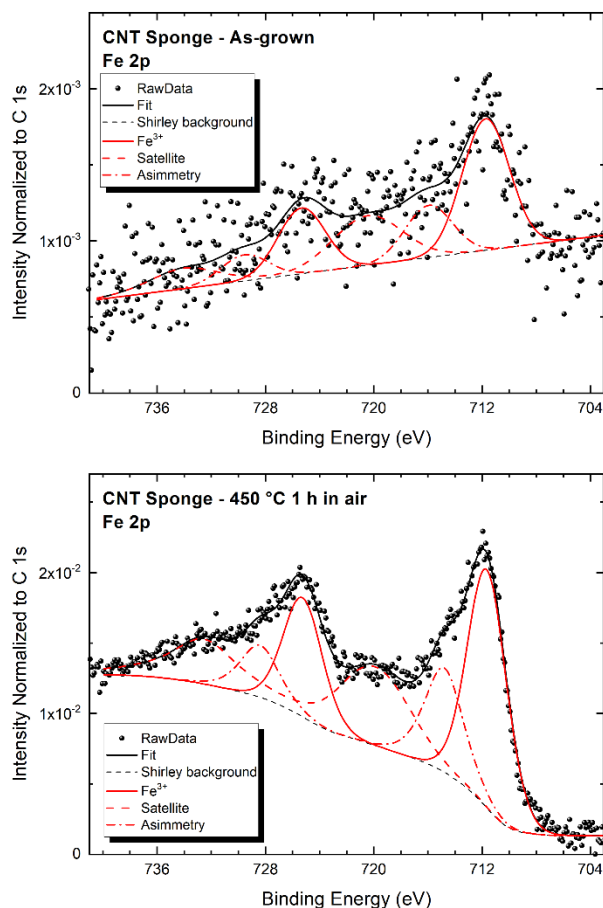
Figure S2. Fe 2p core levels for as-grown (top panel) and thermally treated (bottom panel) CNT sponge. After background subtraction, the fit was performed considering also the satellites due to the oxide and an asymmetry contribution.

Thermal stability of CNT sponges

The thermal stability of CNT sponges has been characterized by thermal gravimetric analysis (TGA) and differential thermal analysis (DTA). The related spectra are displayed in Figure S3.

The sponges are stable up to around 500 °C when the CNTs start to decompose. The sharp peak in the DTA spectrum in the range 715 – 800 °C indicates the transformation of iron into iron oxide. Iron is the catalyst used for CNT sponge synthesis and is present inside the CNT as nanoparticles. Once the CNTs have been degraded, the metal nanoparticles are exposed to air and react with oxygen.
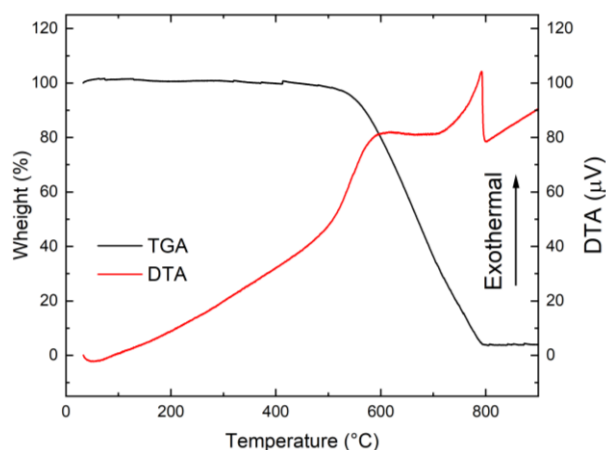
Figure S3. TGA and DTA analyses collected on a piece of CNT sponge weighting 19.0 mg.

Raman analysis of CNT sponges

Both as-grown and thermally-treated CNT sponges have been characterized with Raman spectroscopy. For this analysis, a Labram Micro Raman apparatus by Jobin Yvon was used, with λ=532 nm excitation in backscattering geometry through a 20x long working distance objective and power of 0.5 mW.

The Raman spectra of the two sponges are displayed in Figure S4 for the wavelength region 1100 cm^{-1} to 1800 cm^{-1}. According to literature, five different bands can be found in this region, namely D*, D, D'', G and D'. The D* band has been observed in disordered graphitic structures [1], sp^3-rich phases [2] and alternating chain of sp^2 carbons with a single hydrogen bonded to carbon in nanocrystalline diamond [3]; the D band, peaked here at around 1337 cm^{-1}, arises from defect-assisted double resonant processes near the K point of the Brillouin Zone [4]; the D'' band is related to amorphous carbon phase [5]; the G band is due to the E_{2g} optical phonon [6]; and the D' is ascribed to an intra-valley resonance with the G band and undergoes splitting in the presence of impurities [7].

As a general remark, it can be seen that the Raman spectra of the two sponges in Figure 4S are very similar. For example, in both cases, the D band is the most intense signal, indicating a large amount of defects in the analysed samples. It can be seen, however, that the after annealing at 450 C in air for 1 h, the G and the D' bands (in the range 1500 – 1660 cm^{-1}) become somewhat less intense and less wide maybe due to saturation of some defects in the graphitic lattice of the CNTs with oxygen-containing functional groups.
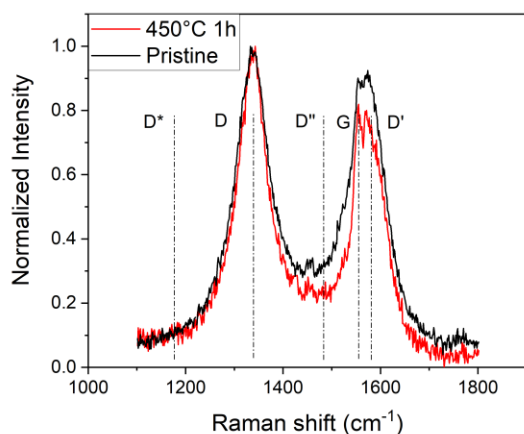
Figure S4. Raman spectra of an as-grown (black curve) and a thermally-treated (red curve) CNT sponge. The spectra have been normalized to the maximum intensity of the D band, peaked around 1337 cm^{-1}.

References
[1] R. Al-Jishi and G. Dresselhaus. *Phys. Rev. B* **26**, 4514 (1982)
[2] R.J. Nemanich et al. *J. Vac. Sci. Technol. A* **6**, 1783
[3] A.C. Ferrari and J. Robertson. *Phys. Rev. B* **63**, 121405 (2001)
[4] S. Reich and C. Thomsen. *Philos. Trans. R. Soc. A Math. Phys. Eng. Sci.* **362**, 2271-2288 (2004)
[5] S. Vollebregt et al. *Carbon* **50**, 3542 (2012)
[6] R. Vidano and D.B. Fischbach. *J. Am. Ceram. Soc.* **61**, 13-17 (1978)
[7] A.C. Ferrari et al. *Phys. Rev. Lett.* **97**, 1-4 (2006)